Influence of expression and purification protocols on Gα biochemical activity: kinetics of plant and mammalian G protein cycles

Running head: G protein biochemical activity *in vitro*

Timothy E. Gookin[1,2], David Chakravorty[1,2] & Sarah M. Assmann[1*]
[1] Biology Department, Pennsylvania State University, University Park, Pennsylvania 16802
[2] These authors contributed equally to the article.

ORCID IDs: 0000-0002-0994-0790 (T.E.G.); 0000-0002-6591-4853 (D.C.); 0000-0003-4541-1594 (S.M.A.).

*Author for correspondence:

Sarah M. Assmann, sma3@psu.edu, 814-863-9579

Abstract

Heterotrimeric G proteins, composed of Gα, Gβ, and Gγ subunits, are a class of signal transduction complexes with broad roles in human health and agriculturally relevant plant physiological and developmental traits. In the classic paradigm, guanine nucleotide binding to the Gα subunit regulates the activation status of the complex. We sought to develop improved methods for heterologous expression and rapid purification of Gα subunits. Using GPA1, the sole canonical Gα subunit of the model plant species, *Arabidopsis thaliana*, we observed that, compared to conventional purification methods, rapid StrepII-tag mediated purification facilitates isolation of protein with increased GTP binding and hydrolysis activities. This allowed us to identify a potential discrepancy with the reported GTPase activity of GPA1. We also found that human GNAI1 displayed increased GTPase activity when purified using our approach, indicating our protocol is applicable to mammalian Gα subunits, potentially including those for which purification of enzymatically active protein has been historically problematic. We then utilized domain swaps of GPA1 and human GNAO1 to demonstrate that the inherent instability of GPA1 is a function of the interaction between the Ras and helical domains. Additionally, we found that GPA1-GNAO1 domain swaps uncouple the instability from the rapid nucleotide binding kinetics displayed by GPA1.

Keywords: Heterotrimeric G protein, GPA1, GNAI1, GNAO1, BODIPY, GTP, StrepII

Introduction

The heterotrimeric G protein complex consists of an alpha (Gα), beta (Gβ), and gamma (Gγ) subunit, in which Gβ and Gγ exist as a non-dissociable dimer. Heterotrimeric G proteins (G proteins) are well-studied conserved eukaryotic signal transduction components. Mutations of G protein subunits in humans have been associated with diseases and developmental abnormalities including cancer (1-3), neurodevelopmental disorders (4), McCune-Albright Syndrome (5), diabetes (6, 7), hypertension (8) and ventricular tachycardia (9). In plants, null mutants of G protein subunits have been utilized to implicate G proteins in agronomically important traits such as morphological development (10, 11), grain shape and yield (12), hormone sensitivity (13, 14), stomatal responses (15-17), salinity tolerance (18), drought tolerance (19) and pathogen resistance (20, 21).

The Gα subunit of the G protein heterotrimer binds guanine nucleotides in a binding pocket located within a cleft between the Ras-like and helical domains of the protein. The identity of the nucleotide, GDP or GTP, determines the activation state of the heterotrimer in the canonical signaling paradigm. In the inactive heterotrimer, Gα exists in the GDP-bound form, while stimulation of GTP-binding results in activation of the heterotrimer and dissociation of Gα from the Gβγ dimer. Gα and Gβγ are then able to signal to downstream effectors, until the intrinsic GTPase activity of the Gα subunit hydrolyzes GTP to GDP, thereby stimulating reassociation of the inactive heterotrimer. The activation status of the complex can be regulated by guanine

nucleotide exchange factors (GEFs) including 7-transmembrane spanning G protein-coupled receptors (GPCRs) that stimulate GTP-binding, and GTPase activating proteins (GAPs) such as regulator of G protein signaling (RGS) proteins that stimulate GTP hydrolysis (22). In mammals the GPCR superfamily is large and perceives diverse ligands, with over 800 GPCRs encoded in the human genome (23). In contrast, only a few 7TM proteins have been identified as candidate GPCRs in plants (24, 25), including in the intensively studied model dicot *Arabidopsis thaliana* (26). Instead, receptor-like kinases (RLKs) may predominate in the GPCR role in plants (17, 27-31).

Here, we sought to assess the kinetics of the sole canonical Arabidopsis Gα subunit, GPA1, in comparison with two closely related mammalian G proteins in the $G\alpha_{i1}$ family, GNAI1 and GNAO1. GPA1 has previously been described to: i) display self-activating properties due to spontaneous nucleotide exchange and fast GTP-binding, and ii) exhibit slow GTPase activity, which skews the protein to the GTP-bound form, especially when compared to the human $G\alpha_{i1}$ protein, GNAI1 (32, 33). However, in the course of our investigations, we found that specific purification protocols and protein storage impair the activity of both plant and mammalian Gα proteins.

Purification of active recombinant heterotrimeric G protein Gα subunits is integral to understanding structure-function relationships. Jones et al. (32) determined the structure of GPA1 by x-ray crystallography, discovering that the GPA1 tertiary structure bears a strong resemblance to that of GNAI1. Yet, GPA1 and GNAI1 also display distinctly different enzymatic activities, indicating that differences arise on a finer scale, possibly due to high levels of intrinsic disorder within, and dynamic motion of, the GPA1 helical domain (32). Therefore, we developed a robust expression and rapid purification protocol utilizing dual StrepII-tags (34), which allowed for elution in a buffer directly compatible with downstream BODIPY-GTP/-GDP binding assays, thereby abrogating any need for protracted buffer component removal, e.g. by dialysis. GPA1 exhibits increased activity when rapidly purified using a specific purification protocol. Furthermore, comparison with the two human Gα subunits from the $G\alpha_i$ family demonstrated that mammalian Gα activity is also impacted by the choice of purification regime, and that our StrepII-tag approach to expression and purification can improve the activity of some mammalian Gα subunits.

Results

Rapid purification of recombinant GPA1 yields higher activity *in vitro*

The dual StrepII tag consists of tandem StrepII tags separated by a flexible linker. The original Strep tag was identified as a streptavidin binding tag that could be used to isolate recombinantly expressed antibodies (35). Both the Strep tag as well as streptavidin were further engineered to form a StrepII-Streptactin system with increased affinity, and the ability for N-terminal and C-

terminal tagging (36, 37). As the resin conjugated Streptactin used to purify StrepII-tagged proteins exists in a tetrameric state, the use of two tandem StrepII tags separated by a linker was subsequently employed to further increase binding affinity via the avidity effect while still allowing efficient competitive elution (36) in a buffer compatible with many *in vitro* assays. We therefore utilized dual N-terminal StrepII tags separated by a linker sequence (SGGSGTSGGSA), similar to the linker used in the Twin-Strep-tag (GGGSGGGSGGSA) (36), to purify GPA1, the sole canonical Gα subunit from Arabidopsis. We adapted the base pGEX vector backbone to include N-terminal dual-StrepII tags, thrombin and TEV protease sites, a multiple cloning site, and the option of a C-terminal FLAG tag in a new vector we named pSTTa. GPA1 expressed from pSTTa was purified and observed to be highly pure (Figure S1A). In a classic *in vitro* assay, fluorescent signal increases as Gα proteins bind BODIPY-conjugated GTP and decreases when GTP hydrolysis outpaces GTP binding, due to resultant partial fluorophore re-quenching (38-43). After numerous trials of multiple growth and induction protocols, we found that use of BL21 (DE3) cells cultured in high salt LB (HSLB) media resulted in the highest yield of StrepII-GPA1, so we utilized HSLB for growth and induction in all subsequent experiments. We found that freshly purified GPA1 exhibits a characteristic BODIPY-GTP kinetic curve indicative of rapid GTP binding and rapid GTP hydrolysis but GPA1 assayed after overnight storage at 4 °C, a proxy for standard buffer dialysis protocols, shows reduced GTP binding with slower kinetics (Figure 1A). To circumvent the detrimental overnight dialysis step, we prepared His-GPA1 and GST-GPA1 fusion proteins fresh and as rapidly as possible, utilizing 10 kDa molecular weight cut-off centrifugal filter units for post-elution buffer exchange into “EB Base”, the buffer used for StrepII-GPA1 elution but lacking desthiobiotin. When purified side-by-side with StrepII-GPA1, the buffer exchange steps applied to the His-GPA1 and GST-GPA1 proteins added approximately 45 minutes of additional handling, which was performed on ice and in a 4 °C refrigerated centrifuge, while the StrepII-GPA1 sample was kept on ice. When separated by SDS-PAGE, the StrepII-GPA1 protein was obviously more pure than the His-GPA1 or GST-GPA1 preparations under these rapid purification conditions (Figure S1B). Despite comparable affinity purification protocols and rapid handling at cold temperatures for the post-purification buffer exchange steps, the His-GPA1 and GST-GPA1 proteins displayed lower apparent binding and hydrolysis activities than the StrepII-GPA1 protein (Figure 1B). As peak fluorescence of BODIPY-GTP is a function of net binding and hydrolysis, another interpretation for the lower activity observed for His- and GST- fusions in Figure 1B is that GTP binding rate is unaltered between the proteins, but GTP hydrolysis is faster in the His- and GST-fusions. We therefore assayed binding to the non-hydrolyzable BODIPY-GTPγS using rapid sampling in well mode for 30 seconds to assess the initial relative GTPγS-binding rates. Indeed the StrepII-GPA1 protein displayed appreciably faster BODIPY-GTPγS binding compared to the His-GPA and GST-GPA1 preparations (Figure 1C), consistent with the interpretation that the StrepII-GPA1 preparation displays higher activity.

One possible explanation for the increased apparent activity of the StrepII-GPA1 protein compared to His-GPA1 and GST-GPA1 (Figure 1B) is that a co-purifying contaminant in the StrepII-GPA1 preparations displays GTP-binding and hydrolysis activities. Though the StrepII purifications commonly yield highly pure protein, we almost always observed a minor contaminating band slightly larger than 70 kDa in our GPA1 elutions (Figure S1A). To verify the

lack of GTP binding by any co-purifying contaminant, we expressed and purified a GPA1^{S52N} mutant that, as observed previously for a GPA1^{S52C} mutant (41), does not bind GTP. StrepII-GPA1^{S52N} displayed no BODIPY-GTP or BODIPY-GTPγS-binding activity (Figure S1C and D), confirming that the binding and hydrolysis observed for StrepII-GPA1 was solely a result of GPA1 activity. Mass spectrometric identification was performed on the 70+ kDa protein and it was found to correspond to *E. coli* DnaK, which is not expected to display GTP binding activity (44).

GPA1 stability

To investigate the underlying cause of *in vitro* GPA1 activity loss, we assessed GPA1 conformational stability utilizing SYPRO Orange fluorescence. SYPRO Orange fluorescence increases upon interaction with hydrophobic regions of the protein, which will have greater accessibility upon protein unfolding. We observed that at our standard BODIPY-GTP binding assay temperature of 25 °C, GPA1 protein displayed a steady increase in SYPRO Orange fluorescence over the course of 30 min, indicative of protein unfolding (Figures 1D and E). Therefore, for future assays we stored GPA1 and other Gα proteins for matched assays on ice in a 4 °C refrigerator during post-elution quantification steps, prepared reaction mixes on ice, and allowed no more than 2 minutes of temperature equilibration for samples immediately prior to initiating assays, to mitigate loss of activity.

Incubation of GPA1 with excess unlabelled GDP (Figure 1D) or GTPγS (Figure 1E) restored protein stability while allowing for nucleotide exchange assessment, yet GDP inclusion also appears to compete with BODIPY-GTP/-GTPγS for binding under reaction conditions. For example, we found that inclusion of GDP in the cell lysis and binding buffer allowed for pre-loading of GPA1 with GDP, presumable short-term protein stabilization, and increased BODIPY-GTPγS binding activity (Figure S1E). By contrast, inclusion of GDP in the lysis and elution buffers resulted in protein with decreased BODIPY-GTPγS binding (Figure S1E); presumably the lower apparent binding equilibrium is due to an excess of unlabeled GDP competing with BODIPY-GTPγS for binding to GPA1.

Given the stability issues of GPA1 outlined above, we wondered if storage at -80 °C and freeze-thawing also has an impact on GPA1 activity. Therefore we purified StrepII-GPA1 and added either an additional 10% glycerol or 8.33% sucrose as a cryoprotectant (45), snap froze the protein with liquid N_2 and stored the proteins for three weeks at -80 °C. Upon thawing and assaying the protein we observed that GPA1 frozen with sucrose as a cryoprotectant displayed more rapid BODIPY-GTP binding and faster hydrolysis than GPA1 frozen with glycerol. This difference suggests the standard use of glycerol as a cryoprotectant is suboptimal for storage of GPA1. In fact our data indicate the use of glycerol alone as a cryoprotectant could result in an underestimate of the peak net hydrolysis rate of GPA1 by ~55%. The BODIPY-GTP binding and hydrolysis curves of GPA1 frozen with sucrose (Figure 1F) was similar to freshly prepared GPA1, e.g. as observed in Figure 1A. The remaining GPA1 data presented in this paper are results from freshly isolated StrepII-GPA1. Storage supplemented with 8.33% sucrose is a viable alternative approach provided that all proteins to be compared are handled equivalently.

Purification of the RGS1 cytosolic domain

Arabidopsis *RGS1* encodes a protein with seven transmembrane spanning domains at the N-terminus and a cytosolic RGS domain at the C-terminus. Previous assays of RGS1 activity have therefore utilized only the cytosolic RGS domain (46, 47). We recombinantly produced the RGS1 cytosolic domain utilizing the pSTTa vector to confirm; i) that RGS1 is amenable to rapid purification via dual StrepII-tags, and more importantly ii) that the StrepII-tagging approach for GPA1 did not disrupt GPA1 interaction with the primary regulator, RGS1. The addition of StrepII-RGS1 to StrepII-GPA1 in a BODIPY-GTP assay strongly promoted the hydrolysis of GTP by GPA1 (Figure S1F), indicating both i and ii are true.

Comparison of GPA1 to human GNAI1/GNAO1

Arabidopsis GPA1 bears high structural similarity to human GNAI1, which has provided a rationale for previous biochemical comparisons of GPA1 with GNAI1 (32). We therefore sought to reexamine this comparison utilizing our newly optimized recombinant GPA1 purification protocol. We cloned GNAI1 into pSTTa using both codon harmonized (GNAI1ch) and wild-type (GNAI1wt) sequence (Figures S2A and B). We found that proteins derived from the two constructs were essentially interchangeable as side-by-side comparisons showed the GNAI1wt and GNAI1ch proteins did not differ in yield or purity (Figure S2C), in BODIPY-GTP binding and hydrolysis (Figure S2D), or in BODIPY-GTPγS binding (Figure S2E). For a human Gα contrast with GNAI1, we prepared a construct for another human $G\alpha_i$ subfamily member, GNAO1, which has been shown to display considerably faster kinetics than GNAI1 (42). On a sequence level, the GNAI1 protein shares 38.2% identity and 56.8% similarity with GPA1, while GNAO1 displays 37.0% identity and 54.1% similarity with GPA1. Therefore, it is reasonable to compare GPA1 to both of these mammalian $G\alpha_i$ proteins .

We purified StrepII-GNAI1 and StrepII-GNAO1, and compared their wild-type activities to those of their constitutively active mutants (StrepII-GNAI1^{Q204L}/GNAO1^{Q205L} (48)), and to activities of mutants corresponding to the plant nucleotide-free GPA1^{S52N} mutant (StrepII-GNAI1^{S47N}/StrepII-GNAO1^{S47N}). Both wild-type GNAI1 and GNAO1 proteins displayed GTP-binding and hydrolysis activities, and as expected based on previous studies (42), the net GTP binding activity of GNAI1, reflected by the amplitude of peak fluorescence, was considerably lower than that of GNAO1 (Figures 2A and B). The constitutively active mutants (Q204L/Q205L) displayed slower binding than the wild-type proteins and no hydrolysis activity, as expected, while the S47N mutants displayed no BODIPY-GTP binding activity (Figures 2A and B). Surprisingly, the S47 mutants both displayed BODIPY-GTPγS binding activity that occurred faster than was observed for the wild-type GNAI1 and GNAO1 proteins (Figures 2C and D). The binding activity was, however, transient with a peak observed at 3-4 minutes, followed by a steady decline in signal. The decline is unlikely to be due to hydrolysis as GTPγS is considered non-hydrolysable, and no evidence of BODIPY-GTPγS hydrolysis was evident in any of our assays with wild-type GNAI1 or GNAO1. These results are in contrast to the analogous GPA1^{S52N} mutant, which displayed no BODIPY-GTPγS binding (Figures S1C and D).

The S47 residue within the G1 motif is important for Mg^{2+} cofactor coordination (49) and since other metal ions are known to inhibit Gα nucleotide binding (50), we routinely utilized trace-metal-free (TMF) grade components to standardize our assays, which explicitly ruled out any effect of extraneously-present divalent ions, including Mg^{2+}. Notably, we also show that TMF components are not necessary for basic assays, and our methodology can be performed using standard grade reagents (Figure S2F). The GNAI1^{S47N} and GNAO1^{S47N} mutants retain some ability to bind BODIPY-GTPγS, unlike GPA1^{S52N}; yet, without proper coordination of the Mg^{2+} cofactor, this binding is transient (Figures 2C and D). Given that the BODIPY fluorophore is covalently attached differently in BODIPY-GTP (ribose ring) and BODIPY-GTPγS (γ-phosphate), inconsistencies in binding results between the two BODIPY reagents could arise from a combination of steric differences of the binding pocket between mutants and the respective locations of the BODIPY fluorophore. To check if the S47N mutants do retain some residual Mg^{2+} binding, we performed BODIPY-GTPγS binding assays ±Mg^{2+}. In our ±Mg^{2+} assay, both wild-type GNAI1 and GNAO1 displayed a clear requirement for Mg^{2+}, with a very low level of BODIPY-GTPγS binding activity observed in the absence of Mg^{2+} (Figures 2E and F). Similarly, in the S47N mutants the more rapid but transient binding of BODIPY-GTPγS was only observed in the presence of Mg^{2+} (Figures 2E and F), confirming a requirement for Mg^{2+} for in guanine nucleotide coordination. To rule out impairment of the S47N mutant due to protein storage we prepared fresh StrepII-GNAO1 and StrepII-GNAO1^{S47N} to repeat the BODIPY-GTPγS binding assay seen within Figure 2D and 2F. In this instance we assayed BODIPY-GTPγS binding over the first 10 minutes to focus on the shift from rapid to transient binding by StrepII-GNAO1^{S47N}. The fresh and frozen proteins displayed the same trend, including the rapid but transient StrepII-GNAO1^{S47N} BODIPY-GTPγS binding (Figure 2G), ruling out protein storage as a confounding factor. We then investigated protein instability as the potential underlying cause for the transient BODIPY-GTPγS binding by StrepII-GNAO1^{S47N}. A SYPRO Orange assay comparing fresh StrepII-GNAO1 to StrepII-GNAO1^{S47N} demonstrated that the mutant did not exhibit appreciably more protein unfolding within the 30 min assay conditions (Figure 2H), as the curves of wild-type and mutant GNAO1 displayed a similar shape. However, the GNAO1^{S47N} protein did display a different basal level of SYPRO Orange fluorescence, even in the presence of additional GTPγS (Figure 2H). This difference between the wild-type and mutant GNAO1 may indicate a difference in protein conformation, which could be reflected in the different abilities of BODIPY-GTP vs. BODIPY-GTPγS to bind to GNAO1^{S47N} (Figure 2B vs. 2D). Taken together, these data suggest GNAI1^{S47N} and GNAO1^{S47N} do retain some affinity and requirement for Mg^{2+}, though weaker Mg^{2+} coordination is expected. The transient nature of the BODIPY-GTPγS binding may reflect transient Mg^{2+}-binding rather than protein instability.

Next we compared the binding activities of StrepII-GPA1 to StrepII-GNAI1 and StrepII-GNAO1. StrepII-GNAI1 displayed a much lower apparent BODIPY-GTP binding peak than StrepII-GPA1, while StrepII-GNAO1 displayed an intermediate activity (Figure 3A). As peak fluorescence reflects a net activity of GTP binding and hydrolysis, these initial results were consistent with GPA1 displaying a faster binding and slower hydrolysis rate than GNAI1, however, interpretation of the comparison to GNAO1 was less clear. As the StrepII purification protocol was superior to His purification for GPA1, we characterized StrepII-tagged GNAI1 and GNAO1 in comparison to the commonly used His-tagged GNAI1 and GNAO1. We found optimal tags

and purifications differed not just between human Gα subunits and Arabidopsis GPA1, but also between the human Gα subunits. His-GNAI1 and StrepII-GNAI1 displayed similar binding profiles in the initial minutes of the BODIPY-GTP assay, yet His-GNAI1 displayed almost no GTP hydrolysis activity while StrepII-GNAI1 displayed a clear transition to net hydrolysis within three minutes (Figure 3B). The hydrolysis result indicates that StrepII purification is a superior protocol for GNAI1. By contrast, His-GNAO1 displayed higher net BODIPY-GTP binding and hydrolysis activities than StrepII-GNAO1 (Figure 3C), and the difference was just as clear for binding of BODIPY-GTPγS (Figure 3D), indicating the His purification protocol is the more appropriate method to assay GNAO1 activity.

Given the above results, we performed side-by-side purifications of StrepII-GPA1 and His-GNAO1, which demonstrated that GPA1 does indeed display a faster GTP binding rate than GNAO1, but the net hydrolysis rates appear to not to be as different between plant and human Gα subunits as previously thought (Figure 3E). To isolate the observed binding rate of the Gα proteins, we performed an analogous assay with the non-hydrolyzable BODIPY-GTPγS. Indeed the initial rate of BODIPY-GTPγS binding to GPA1 was more rapid than to GNAO1, yet the GPA1 maximal binding signal was unexpectedly much lower than GNAO1, and rather than plateau as with GNAO1, the GPA1 BODIPY-GTPγS signal decreased over time (Figure 3F). Possible reasons for the difference in signal maxima include: i) steric differences of the Gα binding pockets resulting in differential levels of BODIPY fluorophore unquenching upon protein binding, and ii) inherent instability of GPA1 resulting in a lower apparent binding activity *in vitro*. We believed hypothesis i) was unlikely as the empirically derived crystal structures of GPA1 and GNAO1 are highly similar (Figure S3A), just as are the structures of GPA1 and GNAI1 (Figure S3B). We therefore sought to assess the amount of each enzyme necessary to observe saturated and stable binding of 50 nM BODIPY-GTPγS, as a reflection of Gα activity retained *in vitro*. Despite being in excess, 100 nM, 200 nM and 400 nM concentrations of StrepII-GPA1 were unable to attain a maximal binding signal with 50 nM BODIPY-GTPγS. Only 800 nM or 1.2 µM GPA1 displayed a stable binding plateau at the maximal level (Figure 3G). In comparison, all concentrations of GNAO1 either attained a maximal plateau, or neared maximal fluorescence in the case of 100 nM GNAO1, within the course of our assay (Figure 3H). The necessity for higher GPA1 concentrations in reaching binding saturation reflects the established lower stability of GPA1 *in vitro* (Figures 1 D and E), but also provides insight to the GNAO1>GPA1 signal maxima in Figure 3F. Notably, the maximal levels of BODIPY-GTPγS fluorescence were quite similar between high concentrations of GPA1 and GNAO1 when assayed side-by-side (Figures 3G and 3H), thereby refuting hypothesis i) above by indicating that steric differences in the binding pockets do not result in different levels of BODIPY fluorophore unquenching. Next we compared the ability of excess (10 µM) GDP to suppress binding of 50 nM BODIPY-GTP to 100 nM Gα proteins (Figure 3I). BODIPY-GTP binding by GPA1 was partially suppressed by 10 µM GDP, but almost completely abolished for GNAO1. The striking difference in GDP suppression of GTP binding likely reflects a higher relative affinity for GTP than GDP and significantly faster nucleotide exchange rate of GPA1 than GNAO1.

GPA1-GNAO1 helical domain swaps

It has been proposed that the helical domain of GPA1 displays a marked level of intrinsic disorder and increased dynamic motion compared to that of GNAI1 (32). Jones et al. (32) confirmed that a helical domain swap between GPA1 and GNAI1 largely swapped the relative kinetics between the two Gα proteins. In those studies, the GPA1 helical domain conferred rapid spontaneous activation to GNAI1 while the GNAI1 helical domain conferred slower activation to GPA1. We wondered if a helical domain swap between GPA1 and GNAO1 would: i) display as strong a difference as the GPA1-GNAI1 domain swap, and ii) confirm that the helical domain of GPA1 is responsible for the poor stability of GPA1. Therefore, we created our reciprocal domain swap constructs GPA1^{GNAO1hel} (GPA1 Ras domain fused to the GNAO1 helical domain) and GNAO1^{GPA1hel} (GNAO1 Ras domain fused to the GPA1 helical domain). To not confound any tag/purification effects with the domain swap effects, we utilized our StrepII tagging and purification methods for all proteins. A comparison of BODIPY-GTPγS binding demonstrated that binding rates increased in the following order: GNAO1<GPA1^{GNAO1hel}<GPA1<GNAO1^{GPA1hel}. Beyond this initial binding rate, GPA1 displayed the lowest signal amplitude corresponding to peak binding, while GNAO1^{GPA1hel} displayed the highest signal plateau (Figure 4A). In BODIPY-GTP assays, which integrate GTP binding and hydrolysis, the same initial trend was largely displayed during the binding phase, GNAO1<GPA1^{GNAO1hel}=GNAO1^{GPA1hel}<GPA1 (Figure 4B). Once BODIPY-GTP hydrolysis exceeded the binding rate, we observed the following order of maximal net hydrolysis rates: GNAO1<GPA1^{GNAO1hel}<GNAO1^{GPA1hel}<GPA1 (Figure 4B). Therefore, although the rate of GTPγS binding by GNAO1^{GPA1hel} was the fastest of the four proteins assayed, peak BODIPY fluorescent signal was dampened by a rapid switch to hydrolysis. We then assessed the relative conformational stability of the GPA1, GNAO1, GPA1^{GNAO1hel} and the GNAO1^{GPA1hel} proteins in a SYPRO Orange assay ±10 μM GTPγS (no BODIPY label). As suspected, the GNAO1 helical domain conferred a similar stability to GPA1 as did excess GTPγS (Figures 4C and D). As before, GPA1 samples without nucleotide supplementation displayed increased SYPRO Orange signal indicative of protein unfolding, and was the only protein in the domain swap assays to display considerable divergence between the ±GTPγS samples (Figures 4C and D). Interestingly, at “T=0” of the SYPRO Orange assay the fluorescence of GPA1 in the absence of nucleotide supplementation was already much higher than that of most other samples. We note that all of these samples were prepared on ice in duplicate, pipetted into the assay plate and loaded into the plate reader; a process that took ~4 minutes for the number of samples in Figures 4C and D. To investigate the difference at “T=0” of the assays comparing multiple samples, we performed a 1 vs. 1 assay comparing single wells of GPA1 vs. GPA1 +10 μM GDP. This assay can be initiated in seconds and allowed us to monitor SYPRO Orange fluorescence almost immediately after removal from ice. Indeed, in this rapid assay, the initial fluorescence levels were similar between the samples before a steady rise in fluorescence signal was observed in the GPA1 alone reaction (Figure S3C). The initial similarity of fluorescence between ±nucleotide samples was quite similar to the results shown in Figures 1D and E, which were assays run on an intermediate scale compared to the large assay in Figure 4C and small assay in Figure S3C. GNAO1^{GPA1hel} in the large scale assay also displayed a higher initial value of SYPRO Orange fluorescence, and noticeably more signal variation between timepoints. However, unlike GPA1, the addition of GTPγS did not repress the

high fluorescence values at T=0, and the fluorescence signals for GNAO1^{GPA1hel} did not rise as obviously through the assay as they did for GPA1 in the absence of GTPγS (Figures 4C and D). These traits appear consistent with GNAO1^{GPA1hel} achieving a stable but different conformation than the other Gα proteins assayed in Figure 4; a conformation that is seemingly characterized by increased surface accessibility of hydrophobic residues for SYPRO Orange binding. In summary, for GPA1 *in vitro*, unfolding at room temperature and then 25 °C began almost immediately and was evident on a scale of seconds to minutes, further underscoring the need to use a rapid purification protocol. Interestingly, our domain swap assays indicate that neither the Ras nor the helical domain alone accounts for the lack of stability.

Discussion

Purification of functional recombinant heterotrimeric G protein Gα subunits is integral to understanding their roles in both animals and plants. The former is of importance due to their well-described functions in human health (51), and the latter is important due to G protein involvement in controlling agriculturally important traits (12). We demonstrate for the Arabidopsis Gα subunit, GPA1, that protracted handling and/or storage using the standard protocol of glycerol as a cryoprotectant are detrimental to isolating optimally functional protein (Figure 1). Therefore we developed a StrepII-tag purification protocol that allowed rapid on-column binding to isolate highly pure protein for immediate downstream analyses. The utilization of an elution buffer compatible with downstream assays, abolishing the need for buffer exchange steps, is a major advantage for the StrepII purification protocol. Even with the rapid StrepII purification protocol, our data were consistent with some loss of GPA1 activity during the purification and assay timeframe, based on the high concentrations of GPA1 required to saturate binding of 50 nM BODIPY-GTPγS, and the BODIPY signal rundown observed at lower concentrations of GPA1 (Figure 3G, compared to GNAO1 in Figure 3H). Nonetheless, matched purifications demonstrated that the loss of activity for StrepII-GPA1 was substantially less than that observed for commonly used tags: His-GPA1 or GST-GPA1 (Figure 1B). It should be noted that inclusion of GDP in the binding buffer can lead to greater stabilization of GPA1 activity (Figure S1E), presumably by preloading the protein with GDP during lysis and column-binding. Yet, inclusion of GDP in elution or storage fractions is not optimal when assaying intrinsic binding activity as, in the case of GPA1, excess concentrations of GDP can compete with GTP for binding to Gα (Figure S1E).

As our method proved to be an improvement over existing protocols for GPA1 purification (Figure 1B), we applied it to the purification of two closely related human Gα subunits, GNAI1 and GNAO1. We show our method is also applicable to human Gα subunit expression and purification, as demonstrated by the increased GTPase activity observed for StrepII-GNAI1 compared to His-GNAI1 (Figure 3B). We therefore establish StrepII-mediated purification as an addition to the toolkit of possibilities for recombinant investigation of G proteins. However, His-GNAO1 outperformed StrepII-GNAO1 (Figure 3C), reinforcing that tag choice is not universal, and should be optimized for each protein of interest.

We then utilized our newly improved purification protocol to address the following four questions of interest. 1) Does GPA1 indeed display self-activating properties? 2) Is the balance of GTP-loading of GPA1 further skewed to the active state by slow GTP hydrolysis? 3) What are the functional consequences of mutations to the serine residue important for Mg^{2+} ion coordination in the active site? 4) Given that GNAO1 displays rapid enzyme kinetics compared to GNAI1, but without the loss of stability observed in GPA1, can we employ a domain swap approach between GPA1 and GNAO1 to assess the relative contributions of the Ras vs. helical domains to enzyme function and stability? As GPA1 was sensitive to differences in handling, in all assays containing GPA1 we only directly compared proteins prepared fresh side-by-side, and we recommend that as the best practice.

Re-evaluation of GPA1 enzymatic kinetics

Jones et al. (32) characterized GPA1 as a self-activating Gα protein due to rapid GDP release followed by rapid GTP binding. They also reported slow GTP hydrolysis kinetics. Urano et al. (33) followed this study with confirmation that Gα subunits from evolutionarily distant branches of the plant kingdom also exhibit these properties. However, both studies utilized His-tag purification protocols; Jones et al. purified Gα proteins using a 90 min batch binding step with post-elution processing steps and compared GPA1 to the slow GNAI1 protein, and Urano et al. stored purified Gα subunits at -80 °C with glycerol as a cryoprotectant. Though these are standard protocols for Gα purification, with hindsight we suggest these steps are not optimal for isolation of active GPA1. It should also be noted that both studies included GDP in their elution buffers, which assists in GPA1 stabilization (Figures 1D and S1E) but, depending on concentration, can slow GTP binding and therefore the maximal observable hydrolysis rate (Figure 3I). As a result we sought to reassess the conclusions drawn from these studies by utilizing our newly developed rapid Gα purification protocol.

All of our data are consistent with the original assertion that GPA1 displays rapid GTP binding (Figures 1A-C, S1C-F). Even when compared to GNAO1, which displays much faster binding than GNAI1 (Figure 2), GPA1 clearly displays a faster comparative rate of GTP binding (Figures 3E and F). Furthermore, our analyses of GPA1 stability *in vitro* (Figures 1D-E, 4C-D and S3C), and the inability of moderately excess concentrations of GPA1 to saturate BODIPY-GTPγS-binding, suggests that this assessment of GTP binding is still an underestimate due to loss of function during the assay. We also found that storage of GPA1 with glycerol as the only cryoprotectant resulted in an underestimation of GTPase activity (Figure 1F). Specifically, the peak net hydrolysis rate was 55% lower for samples stored with glycerol compared to samples stored with sucrose, which would certainly skew the extent to which GPA1 would be estimated to be GTP loaded. Additionally, the comparison to GNAO1 reveals GPA1 to be less of an outlier than the comparison to GNAI1 would suggest. The apparent peak net hydrolysis rate of GPA1 is 12.5% higher than that of GNAO1, as determined by BODIPY-GTP signal decreases across a 30 second moving window in Figure 3E, indicating relatively similar levels of activity. With regard to spontaneous nucleotide exchange, our data in Figure 3I are particularly compelling. In that GDP competition assay, GDP was provided at 10 μM, i.e. 100x in molar excess of the Gα proteins and 200x in molar excess of BODIPY-GTP. This massive overabundance of GDP was

sufficient to completely outcompete BODIPY-GTP binding by GNAO1 (Figure 3I), reflecting the crucial role of GPCR-mediated stimulation in nucleotide exchange for animal Gα subunits (52, 53). Contrastingly, 10 µM GDP was only partially able to suppress GPA1 BODIPY-GTP binding activity (Figure 3I), consistent with GPA1 displaying a spontaneous nucleotide exchange activity and relatively much higher affinity for GTP than GDP (32, 33, 54). Overall, our data indicate that GPA1 does display rapid properties of both nucleotide exchange and GTP binding, but there likely has been underestimation of GTP hydrolysis activity in the past due to choice of purification protocol. Side-by-side comparisons with two closely related mammalian Gα proteins, all isolated under optimal conditions (Figures 3A and E), reveals that the GTP hydrolysis rate of GPA1 falls within the range of that observed for the animal Gα subunits.

GNAI1^{S47N} and GNAO1^{S47N} mutants display transient GTP binding

With the advent of affordable mass patient genetic testing, a number of mutations of the equivalent sites to GNAI1^{S47}/GNAO1^{S47} and GNAI1^{Q204}/GNAO1^{Q205} of multiple Gα subunits have been associated with various medical conditions in ClinVar (55) and Catalogue Of Somatic Mutations In Cancer (COSMIC) (56) databases, as summarized in Tables S1 and S2, respectively. The Q204/Q205 site resides within the G3 motif (one of five G box motifs important for nucleotide binding) of Gα subunits, mutations of which are well-known to impart a constitutively active status upon Gα proteins (48). Mutations at this site specifically in *GNAQ* and *GNA11* are strongly linked to uveal melanoma (1, 57). The S47 site is relatively less well-understood, though it is a crucial residue within the G1 motif involved in Mg^{2+} cofactor coordination (49). Mutants of S47 and equivalent sites in G proteins have been used as tools of functional investigation before disease associations were identified for the site. For example, an equivalent mutant to S47N in the small monomeric G protein Ras, S17N, was characterized as displaying a 23,000-fold reduction in affinity for GTP (58). Subsequently, a S47C mutation was identified in a random mutagenesis screen of GNAO1 as a protein with low to no GTPγS binding activity (59). In other examples, a $G\alpha_T$ protein in which a region or subregions of amino acids 215-295 have been replaced with the equivalent GNAI1 residues to facilitate expression and purification, has been utilized and named $G\alpha_T$*. When assaying binding of radiolabeled GTPγS by $G\alpha_T$* chimeric proteins, there was an apparent discrepancy between the results of Natochin et al. (60) who reported the S43N and S43C mutants failed to bind GTP, and Ramachandran and Cerione (61) who reported a faster rate of spontaneous GDP-GTPγS exchange for the $G\alpha_T{*}^{S43N}$ mutant compared to $G\alpha_T$*. Our reassessment with real-time BODIPY-GTPγS binding suggests a mechanism by which the discrepancy may be understood. Figures 2C-G indicate the initial rate of BODIPY-GTPγS binding is faster for GNAI1^{S47N} and GNAO1^{S47N} than the respective wild-type proteins, and is Mg^{2+}-dependent. However, the binding is only transient, as shown by the observation that BODIPY-GTPγS signal initially increased, but then gradually decreased 3-4 minutes after binding initiation (Figures 2C and D), a phenomenon that was not explained by protein instability (Figure 2H). Thus, the binding signal could be missed and/or washed off if the protein is subjected to protracted handling in a radiolabeled GTPγS binding assay, which may account for the previously reported GTP-binding discrepancy. Our results provide additional insight into the mechanism by which S47 and equivalent position mutations of

human Gα subunits manifest in disease states. Moreover, our results suggest an advantage of BODIPY assays in facile revelation of real-time kinetics.

GPA1 instability is conferred by combined effects of the Ras and helical domains, and is not inherently linked to rapid nucleotide binding

As mentioned above, studies from the Jones and Dohlman groups have indicated that the GPA1 helical domain displays high levels of intrinsic disorder based on comparisons of the electron density map and atomic displacement parameters of monomers determined by x-ray crystallography, and motion away from the Ras domain as predicted by molecular dynamics simulations (32, 62). Interdomain motion is a mechanism proposed to potentiate nucleotide exchange (52, 53, 63, 64) and therefore these observations for GPA1 are consistent with its status as a Gα subunit capable of spontaneous nucleotide exchange (32). As previously established, a domain substitution using the helical domain of GNAI1 conferred slower nucleotide exchange, faster GTP hydrolysis and increased stability to GPA1. Those stability experiments utilized circular dichroism over a temperature gradient of 15-80 °C, and proteins were assayed in the presence of excess GDP. We however observed using a SYPRO Orange fluorescence assay, that when incubated at 25 °C in the absence of additional nucleotides, GPA1 displayed reduced stability (Figures 1D-E and S3C). We also observed the enzymatic differences between GPA1 and GNAO1 were less than those between GPA1 and GNAI1 (Figure 3), though GNAO1 was likely more stable than GPA1 based on the plateau in BODIPY-GTPγS binding signal observed in Figure 3H. It was intriguing to speculate that the helical domain of GNAO1 may confer stability to GPA1 while also allowing the fast GTP binding kinetics of GPA1 to be retained. Indeed this proved to be the case with $GPA1^{GNAO1hel}$ displaying almost as rapid BODIPY-GTPγS and BODIPY-GTP binding as GPA1 (Figure 4A and B). When protein stability was assayed, we observed that $GPA1^{GNAO1hel}$ displayed a similar resistance to unfolding at 25 °C as GNAO1, distinguishing it from the less stable GPA1 protein (Figure 4C). When provided with a molar excess of GTPγS, GPA1 was as stable as GNAO1 and the two chimeric Gα subunits (Figure 4D).

In the reciprocal domain swap $GNAO1^{GPA1hel}$ displayed rapid BODIPY-GTPγS binding (Figure 4A) and fast hydrolysis (Figure 4B). Unexpectedly, in SYPRO Orange assays $GNAO1^{GPA1hel}$ exhibited a higher basal level of dye interaction than the other Gα proteins, but dye binding did not increase with time, indicating protein stability (Figures 4C and D). As the $GNAO1^{GPA1hel}$ protein also displays strong enzymatic activity (Figure 4A and B), we conclude that the protein is not unfolded, but more likely resides in a stable but alternative conformation to the other Gα proteins assayed. Therefore, as the GPA1 helical domain did not confer instability to GNAO1, we conclude that GPA1 instability is a result of interdomain forces, and that rapid kinetics and instability can be uncoupled by the use of chimeric domain swaps.

Future directions

Our results suggest the need for further evaluation of the GTPase activity of GPA1 in comparison to mammalian Gα subunits. Here we used BODIPY-GTP/-GTPγS to test our newly developed purification approach for GPA1, and screen relative G protein kinetics. We report our purification method as a tool for the community and highlight important contrasts to data from established methods, as well as point to several general consistencies between our data and those of others. We also illustrate an advantage for BODIPY-GTP/GTPγS as it is a real-time method for measurement of direct binding with a sampling rate and processing speed that cannot be matched by traditional radiolabeled nucleotide approaches. These aspects are particularly useful for proteins with rapid kinetics and low stability *in vitro*. However, we also observed one of the major drawbacks of the BODIPY labeling approach in the inconsistency observed between BODIPY-GTP and BODIPY-GTPγS binding for GNAI1^{S47N} and GNAO1^{S47N} (Figures 2A-D). Conjugation of a fluorophore such as BODIPY to GTP can result in differences in apparent binding compared to unlabelled GTP (65, 66), and therefore dictates caution in calculation of absolute rates. Therefore, in the results presented here we limited our calculations to relative rates. While our study demonstrates greater stability *in vitro* for GNAO1 than GPA1, not all human Gα subunits have been as easy to produce recombinantly as GNAO1. For example, chimeric approaches have previously been required to express Gα proteins in the soluble state, including for mammalians Gα subunits such as GNAT1 (61, 67, 68), GNA12 and GNA13 (69). These chimeras integrate short regions of the kinetically particularly slow but easily purified GNAI1 enzyme. Our success with GPA1 purification indicates that our expression and rapid StrepII purification method is worth evaluating for purification of full length recombinant human Gα proteins that are enzymatically active, without the need to resort to chimeric sequence substitutions.

Experimental procedures

Cloning

GPA1 was amplified from *Arabidopsis* cDNA with flanking NcoI and BspEI restriction sites. *GNAI1* with the same flanking restriction sites was amplified from a wild type clone (Genscript, clone OHu13586) and from a designed codon harmonized (70) gBlock synthesized by Integrated DNA Technologies. These Gα subunits were cloned into the NcoI and BspEI sites of pSTTa, a vector we adapted from pGEX to include N-terminal dual-StrepII tags, thrombin and TEV protease sites, a multiple cloning site and an optional C-terminal FLAG tag. *GNAO1* was amplified from a commercial clone (Genscript, clone OHu15183), adapting a 5' BspHI restriction site (yields a sticky end compatible with NcoI) and a blunt 3' end to clone into NcoI/PmlI sites of pSTTa. The C-terminal RGS box of *RGS1* (corresponding to residues 247-459) was amplified from *Arabidopsis* cDNA with flanking NcoI and BspEI sites to clone into pSTTa in the same manner as *GPA1* and *GNAI1*. All genes cloned into pSTTa included a stop codon, so the ORF

did not read through to the C-terminal FLAG tag included in the vector. Mutants of *GPA1*, *GNAI1* and *GNAO1* were generated by REPLACR mutagenesis (71). *GPA1-GNAO1* helical domain swaps were generated by overlap-extension PCR (72) and cloned into pSTTa as above, with the exception that the $GPA1^{GNAO1hel}$ construct was amplified with a 5' BspHI site. Helical domains were defined as GPA1 residues E68-Y188 and GNAO1 residues G63-R177, with the remainder of the protein flanking these regions defined at the Ras domains, consistent with the regions used in the GPA1-GNAI1 domain swap performed by Jones et al. (32). His- and GST-tagged constructs were generated by amplifying the ORFs of *GPA1*, *GNAI1* and *GNAO1*, which were A-tailed, TOPO cloned into pCR8 and mobilized by LR Gateway recombination into pDEST17 (for His-tagged expression), and in the case of *GPA1*, pDEST15 (for GST-tagged expression) (Thermo). Primers for ORF cloning, mutagenesis and overlap-extension PCRs are listed in Table S3. All sequences were verified as correct by Sanger sequencing.

Protein expression

Proteins were heterologously expressed in *E. coli* BL21 DE3 cells using 75 µg/ml carbenicillin for plasmid selection. Typically, fresh transformants were grown in 7.5 ml overnight cultures (LB media supplemented with 0.5% D-glucose (w/v) and 3 g/L $MgCl_{-2}$), pelleted by centrifugation at 5000 g for 10 minutes, and resuspended in 5 ml fresh pre-warmed LB and grown at 37°C. Five ml of pre-warmed HSLB (LB media supplemented with 17 g/L NaCl and 3 g/L $MgCl_{-2}$, pH 7.0) was added at T=20 and 40 min. At T=60 min the pre-culture was added to 600 ml prewarmed HSLB in a vigorously shaking (225 rpm) 2 L baffled flask (OD_{600} = 0.04-0.06). Cultures were grown to an OD_{600} of 0.7-0.8, transferred to a room temperature (20-21 °C) shaker and grown for 20 minutes before induction with 125 µM IPTG for 3-4 hours. Cells were pelleted by 6000 g centrifugation for 10 minutes at 4 °C. Cell pellets were promptly frozen and typically processed the following morning, though proteins retained activity when cell pellets were stored for multiple weeks at -80 °C.

Protein purification

All buffers were prepared with high purity premium grade reagents (e.g. Honeywell TraceSelect, Sigma BioXtra or EMD Millipore EmSure) to minimize introduction of extraneous metals, and supplemented with one tablet Complete EDTA-free protease inhibitor (Roche, 5056489001) or Pierce Protease Inhibitor Tablets, EDTA-free (Thermo, A32965) per 50 ml. Columns were pre-rinsed with 1 ml of 0.25% Tween-20. Frozen cell pellets containing expressed StrepII-tag fusion proteins were resuspended with a 10 ml pasteur pipet in 10 ml buffer W1 (100 mM Tris-HCl, 500 mM NaCl, 2 mM $MgCl_2$, 5 mM TCEP and 5% glycerol pH 8.0) supplemented with ~10 mg lysozyme (Sigma, L1667), 16 µl/ml BioLock biotin blocker (IBA) and 5 µl Pierce Universal Nuclease (Thermo), and kept on ice. Cells were lysed by three rounds of sonication on ice using a Fisher Sonic Dismembrator equipped with a 3 mm tip with 1 second on/off pulses set to 20% amplitude for 15 seconds (i.e. 15x one second pulses), and the cell debris were pelleted by centrifugation at 10000 g at 4 °C for 10-20 minutes. The supernatant was passed through a 0.2 µM PES filter directly into a 10 ml column containing a 0.25 ml resin bed of Streptactin sepharose (IBA) pre-washed with buffer W1. Loaded columns were washed sequentially with

0.5 ml W1 (1x) and 0.3 ml W2 (3x) (50 mM Tris-HCl, 100 mM NaCl and 5% glycerol pH 7.7) before eluting with sequential fractions of 220, 350, and 165 µl of “EB base” (25 mM Tris-HCl, 50 mM NaCl and 5% glycerol pH 7.4) supplemented with freshly added 5 mM desthiobiotin (Sigma) to form “EB”.

For GST-fusion proteins, cell pellets were resuspended in TBS-NoCa binding buffer (50 mM Tris-HCl, 150 mM NaCl, 1 mM MgOAc, 10 mM β-mercaptoethanol and 1 mM Imidazole, pH 8.0) and sonicated and centrifuged as above. The resultant supernatant was passed through a 0.2 µM PES filter into a 10 ml column with a 0.25 ml Pierce Glutathione Agarose (Pierce, 16100) resin bed, essentially mimicking the StrepII purification protocol. Sequential washes were performed with 2 ml (x1) and 1 ml (x2) TBS-NoCa before protein elution with sequential fractions of 220 µl (E1), 350 µl (E2), and 165 µl (E3) TBS-NoCa supplemented with 10 mM glutathione.

His-fusion proteins were purified essentially as previously described for BODIPY reactions (41). Briefly, our purification protocol mimicked the StrepII protocol, with the following modifications: lysis/binding buffer was replaced with 15 ml of 50 mM Tris-HCl pH 8.0, 100 mM NaCl, 2 mM $MgCl_2$, 0.2% $C_{12}E_{10}$, supplemented with 5 µl β-mercaptoethanol post sonication, cell debris was pelleted by centrifugation at 30000 g for 15 min, a 125 µl Talon (Takara) resin bed was used, the resin bed was washed with 1 ml of 50 mM Tris-HCl pH 8.0, 500 mM NaCl, 2 mM MgCl2, 5 mM β-mercaptoethanol, 0.2% $C_{12}E_{10}$ and 10 mM imidazole, and elution was performed with 20 mM Tris-HCl (pH 8.0), 250 mM NaCl, 5 mM β-mercaptoethanol, 10% glycerol and 250 mM imidazole.

Peak elution fractions (second eluate fraction; E2) of GST and His tagged proteins were subjected to buffer exchange using Amicon Ultra 0.5 ml 10 kDa cutoff columns (Millipore Sigma) with five sequential rounds of concentration performed by centrifugation at 14000 g and 4 °C for approximately 10 min and dilution with “EB base” (5x, 5x, 5x, 5x, 2x) for a total dilution of 1250x.

Protein quality and quantity were evaluated immediately after elution by SDS-PAGE of 10-20 µl fractions with a 3-4 lane mass ladder of Fraction V BSA (e.g. 0.5, 1.0, 1.5, 2.0 µg/lane) followed by Gel-Code Blue (Thermo) staining. Biochemical assays were initiated on the fraction displaying peak yield (almost always E2) immediately after PAGE analysis, generally 2-3 hours post-elution, during which time proteins had been stored on ice in a 4 °C refrigerator. Notably, under routine conditions and if pre-quantification of exact yield isn’t critical, the StrepII-tag E2 purity and concentration is consistent enough to allow for immediate biochemical analysis, within minutes of elution.

BODIPY assays

BODIPY-GTP (BODIPY FL GTP - product #G12411) and BODIPY-GTPγS (BODIPY™ FL GTP-γ-S - product #G22183) stocks were purchased from Thermo and diluted to 100 nM in Tris-HCl pH 7.4 immediately prior to use. BSA or buffer alone was used as a negative control as indicated in each assay. Proteins were diluted to twice the final assay concentration, generally 200 nM (GPA1, GNAO1 or BSA) or 400 nM (GNAI1 or BSA) in “EB base” and supplemented

with 10 mM $MgCl_2$ on ice, normally in a master mix sufficient to perform reactions in triplicate. 100 µl of each diluted protein was aliquoted to wells of a Costar 96 well plate (Corning #3631 - black with clear flat bottom non-treated plate) and loaded into a Synergy Neo2 multimode reader (Biotek), or in Figures S1E and F, an Flx800 plate reader (Biotek), set at 25 °C. Pre-injection background readings were taken with monochromators set to 486/18 nm excitation and 525/20 nm emission with a gain setting within the range 90-100 (Synergy Neo2), or 485/20 nm excitation and 528/20 nm emission filters with the sensitivity set to 90 (Flx800). Reactions were initiated utilizing plate reader injectors to dispense 100 µl of BODIPY-GTP or BODIPY-GTPγS to each well (at a rate of 250 µl/sec), yielding a final assay concentration of 50 nM BODIPY-GTP/-GTPγS, 100 or 200 nM protein and 5 mM Mg^{2+} cofactor. Kinetics were normally monitored in "plate mode" for 30 min with a kinetic interval of 3-6 seconds (Synergy Neo2) or 25-30 seconds (Flx800). In cases where rapid monitoring of initial BODIPY-GTPγS binding rates were assayed, samples were monitored in "well mode" for 30 seconds with an 80 msec kinetic interval (Synergy Neo2).

SYPRO Orange assays

We adapted the protein unfolding assay of Biggar et al. (73) to assess protein stability over time at 25 °C. Protein was diluted to 600 nM in "EB Base" supplemented with 5 mM $MgCl_2$ and nucleotides as indicated with 5x SYPRO Orange dye (Thermo #S6650 - 5000X stock). Forty µl per reaction was aliquoted into wells of a FLUOTRAC 200 96 well half area plate (Greiner Bio-One #675076), loaded into a Synergy Neo2 multimode reader (Biotek) and fluorescence was monitored for the indicated length of time with monochromators set to 470/20 nm excitation and 570/20 nm emission with a gain setting of 100 and a kinetic interval of 5 or 6 seconds.

Acknowledgments

We thank Mr David Arginteanu for technical assistance and the suggestion to evaluate sucrose as a cryoprotectant. Supported by NIGMS 5R01GM126079 to SMA. The content is solely the responsibility of the authors and does not necessarily represent the official views of the NIH.

Figure and Table Legends

Figure 1. Fresh StrepII-tagged protein displays higher enzymatic activity than GPA1 proteins purified using other methods or that have been stored. **A.** BODIPY-GTP binding and hydrolysis curves of GPA1 either freshly prepared or subjected to overnight storage at 4 °C to simulate the

temperature and time effect of dialysis. **B.** Comparison of BODIPY-GTP binding and hydrolysis of GPA1 isolated by StrepII-, His- and GST-tag purification procedures. **C.** Comparison of the initial binding rates (note x-axis units) of the samples in panel **B** when assayed with BODIPY-GTPγS. **D-E.** SYPRO Orange protein unfolding assays conducted at 25 °C with GPA1 in the absence of additional nucleotides, compared to GPA1 supplemented with **D.** 125 µM GDP or **E.** 125 µM GTPγS. **F.** Comparison of BODIPY-GTP binding and hydrolysis activities of StrepII-GPA1 stored at -80 °C for 3 weeks with either 10% glycerol or 8.33% sucrose added to the elution fraction (which contains 5% glycerol) as a cryoprotectant. Note: For assays depicted in panels **A** and **F** the detector gain was set to 70, as opposed to 90-100 for other assays, hence the lower relative fluorescence values. 100 nM protein was used in BODIPY assays and 600 nM protein in SYPRO Orange assays.

Figure 2. Comparison of StrepII-GNAI1 and StrepII-GNAO1 with dominant negative (S47N) and constitutively active (Q204L/Q205L) mutants. **A-B.** BODIPY-GTP binding and hydrolysis curves of **A.** GNAI1 or **B.** GNAO1, with corresponding mutants. **C-D.** BODIPY-GTPγS binding curves of **C.** GNAI1 or **D.** GNAO1, with corresponding mutants. **E-F.** Mg^{2+} dependency assays for BODIPY-GTPγS binding by **E.** GNAI1 vs. $GNAI1^{S47N}$ or **F.** GNAO1 vs. $GNAO1^{S47N}$. Note: all proteins assayed in panels **A-F** had been stored at -80 °C with 8.33% sucrose added as a cryoprotectant. **G.** BODIPY-GTPγS binding curves for freshly prepared GNAO1 vs. $GNAO1^{S47N}$ over a 10 min time course. **H.** SYPRO Orange protein unfolding assay of freshly prepared GNAO1 vs. $GNAO1^{S47N}$. Note the expanded y-axis scale. The initial decrease in SYPRO Orange signal may result from temperature equilibration, as reactions were loaded immediately following sample preparation on ice. 200 nM protein was used in GNAI1 and 100 nM protein in GNAO1 BODIPY assays. 600 nM protein was used in the SYPRO Orange assay.

Figure 3. Comparison of GPA1 activity to GNAI1 and GNAO1 activity. **A.** BODIPY-GTP binding and hydrolysis curves of StrepII-GPA1, StrepII-GNAI1 and StrepII-GNAO1. **B-C.** BODIPY-GTP binding and hydrolysis curves of **B.** StrepII-GNAI1 vs. His-GNAI1 and **C.** StrepII-GNAO1 vs. His-GNAO1. **D.** BODIPY-GTPγS binding curves of StrepII-GPA1 vs. His-GNAO1. **E-F.** Comparison of enzyme kinetics of StrepII-GPA1 vs. His-GNAO1. **E.** Binding and hydrolysis of BODIPY-GTP or **F.** binding of BODIPY-GTPγS. **G-H.** Concentration-dependent kinetics and maximal binding of BODIPY-GTPγS by **G.** StrepII-GPA1 or **H.** His-GNAO1. **I.** Comparison of binding and hydrolysis of BODIPY-GTP by StrepII-GPA1 vs. His-GNAO1 ±10 µM GDP. Gα proteins were used at 220 nM in panel B and 130 nM protein in panels C and D, while 100 nM protein was used in panels A, E, F and I.

Figure 4. Helical domain swap between GPA1 and GNAO1. Regions encoding the helical domains of GPA1 (residues 68-188) and GNAO1 (residues 63-177) were reciprocally swapped by overlap-extension PCR and the resultant constructs were all expressed with dual StrepII-tags, to eliminate the tag as a variable. **A-B.** Curves of GPA1, GNAO1 and helical domain swaps for **A.** BODIPY-GTPγS binding and **B.** BODIPY-GTP binding and hydrolysis **C-D.** SYPRO Orange protein unfolding assays conducted at 25 °C with GPA1, GNAO1, $GPA1^{GNAO1hel}$ or $GNAO1^{GPA1hel}$ **C.** in the absence of supplementation with additional nucleotides, or **D.** in the

presence of 10 µM GTPγS. 100 nM protein was used in BODIPY assays and 400 nM protein in SYPRO Orange assays.

Figure S1. Comparison of GPA1 purification methods. **A.** Gel illustrating the purity of StrepII-GPA1 in our protein preparations, with the commonly co-purified 70+ kDa DnaK band. **B.** Proteins were purified in parallel for StrepII-GPA1, His-GPA1 and GST-GPA1 (marked by *) before His-GPA1 and GST-GPA1 proteins underwent buffer exchange into "EB base". Proteins were separated by SDS-PAGE for quantification of yield and qualitative assessment of purity. **C-D.** StrepII-GPA1^{S52N} does not display any binding activity when assayed with **C.** BODIPY-GTP or **D.** BODIPY-GTPγS. **E.** BODIPY-GTPγS binding curves of StrepII-GPA1 supplemented with no GDP, 10 µM GDP in the lysis/binding buffer, or 10 µM GDP in the lysis/binding buffer and elution buffers. **F.** BODIPY-GTP binding and hydrolysis data for 100 nM StrepII-GPA1 ±100 nM StrepII-RGS1 (cytosolic domain). All kinetic data in this manuscript were generated using a Synergy Neo2 multimode reader, with the exception of panels **E** and **F** in this figure, which were generated using an Flx800 plate reader.

Figure S2. Control data for GNAI1 codon harmonization, and buffer reagent choices. **A.** DNA sequence of the codon harmonized GNAI1ch synthesized clone. **B.** Alignment of GNA1wt (native) and GNAI1ch protein sequences, generated with Clustal Omega. **C.** SDS-PAGE illustrates the relative yield and purity of Strep-tag purified GNAI1wt and GNAI1ch proteins. **D-E.** Assays comparing the activities of 250 nM StrepII-GNAI1wt vs. StrepII-GNAI1ch for **D.** BODIPY-GTP binding and hydrolysis, and **E.** BODIPY-GTPγS binding. **F.** Comparison of the BODIPY-GTP binding and hydrolysis activities of 100 nM StrepII-GPA1 purified and assayed in buffers prepared with standard grade reagents or trace metal free (TMF) grade reagents.

Figure S3. A-B. Structural alignments of empirically derived **A.** GPA1-GNAO1 and **B.** GPA1-GNAI1 structures. PDB structure 2XTZ chain A (GPA1 – blue) was aligned in PyMol with 3C7K chain A (GNAO1 – green) or 1GIA chain A (GNAI1 – orange). The nucleotide (yellow for GPA1/light and dark blue for GNAO1 and GNAI1) is located in the binding pocket within the interdomain cleft, which is flanked by the Ras domain (upper domain) and helical domain (lower domain) in both panels. **C.** SYPRO Orange assay with rapid setup of to demonstrate unfolding of GPA1 (600 nM) *in vitro* when not provided with excess nucleotide is almost immediate.

Table S1. Clinvar data associated with equivalent sites to GNAI1^{S47}/GNAO1^{S47} and GNAI1^{Q204}/GNAO1^{Q205} of Gα subunits.

Table S2. COSMIC data associated with equivalent sites to GNAI1^{S47}/GNAO1^{S47} and GNAI1^{Q204}/GNAO1^{Q205} of Gα subunits.

Table S3. Sequences of primers used in this study.

Literature cited

1. Van Raamsdonk, C. D., Bezrookove, V., Green, G., Bauer, J., Gaugler, L., O'Brien, J. M. *et al.* (2009) Frequent somatic mutations of GNAQ in uveal melanoma and blue naevi *Nature* **457**, 599-602
2. O'Hayre, M., Vazquez-Prado, J., Kufareva, I., Stawiski, E. W., Handel, T. M., Seshagiri, S. *et al.* (2013) The emerging mutational landscape of G proteins and G-protein-coupled receptors in cancer *Nature Reviews Cancer* **13**, 412-424
3. Hewitt, N., Ma, N., Arang, N., Martin, S. A., Prakash, A., DiBerto, J. F. *et al.* (2023) Catalytic site mutations confer multiple states of G protein activation *Sci Signal* **16**, eabq7842
4. Muir, A. M., Gardner, J. F., van Jaarsveld, R. H., de Lange, I. M., van der Smagt, J. J., Wilson, G. N. *et al.* (2021) Variants in *GNAI1* cause a syndrome associated with variable features including developmental delay, seizures, and hypotonia *Genet Med* **23**, 881-887
5. Weinstein, L. S., Shenker, A., Gejman, P. V., Merino, M. J., Friedman, E., and Spiegel, A. M. (1991) Activating Mutations of the Stimulatory G Protein in the McCune-Albright Syndrome *N Engl J Med* **325**, 1688-1695
6. Gawler, D., Milligan, G., Spiegel, A. M., Unson, C. G., and Houslay, M. D. (1987) Abolition of the expression of inhibitory guanine nucleotide regulatory protein G_i activity in diabetes *Nature* **327**, 229-232
7. Moxham, C. M., and Malbon, C. C. (1996) Insulin action impaired by deficiency of the G-protein subunit $G_{i\alpha 2}$ *Nature* **379**, 840-844
8. Siffert, W., Rosskopf, D., Siffert, G., Busch, S., Moritz, A., Erbel, R. *et al.* (1998) Association of a human G-protein β3 subunit variant with hypertension *Nature Genetics* **18**, 45-48
9. Lerman, B. B., Dong, B., Stein, K. M., Markowitz, S. M., Linden, J., and Catanzaro, D. F. (1998) Right Ventricular Outflow Tract Tachycardia Due To a Somatic Cell Mutation in G Protein subunit$_{\alpha i2}$ *J Clin Invest* **101**, 2862-2868
10. Ullah, H., Chen, J. G., Young, J. C., Im, K. H., Sussman, M. R., and Jones, A. M. (2001) Modulation of Cell Proliferation by Heterotrimeric G Protein in *Arabidopsis Science* **292**, 2066-2069
11. Ashikari, M., Wu, J. Z., Yano, M., Sasaki, T., and Yoshimura, A. (1999) Rice gibberellin-insensitive dwarf mutant gene *Dwarf 1* encodes the α-subunit of GTP-binding protein *Proc Natl Acad Sci U S A* **96**, 10284-10289
12. Botella, J. R. (2012) Can heterotrimeric G proteins help to feed the world? *Trends Plant Sci* **17**, 563-568
13. Ullah, H., Chen, J. G., Wang, S. C., and Jones, A. M. (2002) Role of a Heterotrimeric G Protein in Regulation of Arabidopsis Seed Germination *Plant Physiol* **129**, 897-907
14. Trusov, Y., Rookes, J. E., Tilbrook, K., Chakravorty, D., Mason, M. G., Anderson, D. *et al.* (2007) Heterotrimeric G Protein γ Subunits Provide Functional Selectivity in G$\beta\gamma$ Dimer Signaling in Arabidopsis *Plant Cell* **19**, 1235-1250
15. Wang, X. Q., Ullah, H., Jones, A. M., and Assmann, S. M. (2001) G Protein Regulation of Ion Channels and Abscisic Acid Signaling in *Arabidopsis* Guard Cells *Science* **292**, 2070-2072
16. Coursol, S., Fan, L. M., Le Stunff, H., Spiegel, S., Gilroy, S., and Assmann, S. M. (2003) Sphingolipid signalling in *Arabidopsis* guard cells involves heterotrimeric G proteins *Nature* **423**, 651-654

17. Yu, Y. Q., Chakravorty, D., and Assmann, S. M. (2018) The G Protein β-Subunit, AGB1, Interacts with FERONIA in RALF1-Regulated Stomatal Movement *Plant Physiol* **176**, 2426-2440
18. Colaneri, A. C., Tunc-Ozdemir, M., Huang, J. P., and Jones, A. M. (2014) Growth attenuation under saline stress is mediated by the heterotrimeric G protein complex *BMC Plant Biol* **14**, 129
19. Ferrero-Serrano, A., and Assmann, S. M. (2016) The α-subunit of the rice heterotrimeric G protein, RGA1, regulates drought tolerance during the vegetative phase in the dwarf rice mutant *d1 J Exp Bot* **67**, 3433-3443
20. Llorente, F., Alonso-Blanco, C., Sanchez-Rodriguez, C., Jorda, L., and Molina, A. (2005) ERECTA receptor-like kinase and heterotrimeric G protein from Arabidopsis are required for resistance to the necrotrophic fungus *Plectosphaerella cucumerina Plant J* **43**, 165-180
21. Trusov, Y., Rookes, J. E., Chakravorty, D., Armour, D., Schenk, P. M., and Botella, J. R. (2006) Heterotrimeric G Proteins Facilitate Arabidopsis Resistance to Necrotrophic Pathogens and Are Involved in Jasmonate Signaling *Plant Physiol* **140**, 210-220
22. McCudden, C. R., Hains, M. D., Kimple, R. J., Siderovski, D. P., and Willard, F. S. (2005) G-protein signaling: back to the future *Cellular and Molecular Life Sciences* **62**, 551-577
23. Hauser, A. S., Attwood, M. M., Rask-Andersen, M., Schiöth, H. B., and Gloriam, D. E. (2017) Trends in GPCR drug discovery: new agents, targets and indications *Nat Rev Drug Discov* **16**, 829-842
24. Gookin, T. E., Kim, J., and Assmann, S. M. (2008) Whole proteome identification of plant candidate G-protein coupled receptors in *Arabidopsis*, rice, and poplar: computational prediction and *in-vivo* protein coupling *Genome Biol* **9**, R120
25. McFarlane, H. E., Mutwil-Anderwald, D., Verbancic, J., Picard, K. L., Gookin, T. E., Froehlich, A. *et al.* (2021) A G protein-coupled receptor-like module regulates cellulose synthase secretion from the endomembrane system in Arabidopsis *Dev Cell* **56**, 1484-1497
26. Urano, D., and Jones, A. M. (2013) "Round Up the Usual Suspects": A Comment on Nonexistent Plant G Protein-Coupled Receptors *Plant Physiol* **161**, 1097-1102
27. Liu, J. M., Ding, P. T., Sun, T. J., Nitta, Y., Dong, O., Huang, X. C. *et al.* (2013) Heterotrimeric G Proteins Serve as a Converging Point in Plant Defense Signaling Activated by Multiple Receptor-Like Kinases *Plant Physiol* **161**, 2146-2158
28. Bommert, P., Il Je, B., Goldshmidt, A., and Jackson, D. (2013) The maize Gα gene *COMPACT PLANT2* functions in CLAVATA signalling to control shoot meristem size *Nature* **502**, 555-558
29. Ishida, T., Tabata, R., Yamada, M., Aida, M., Mitsumasu, K., Fujiwara, M. *et al.* (2014) Heterotrimeric G proteins control stem cell proliferation through CLAVATA signaling in *Arabidopsis EMBO Rep* **15**, 1202-1209
30. Aranda-Sicilia, M. N., Trusov, Y., Maruta, N., Chakravorty, D., Zhang, Y. L., and Botella, J. R. (2015) Heterotrimeric G proteins interact with defense-related receptor-like kinases in *Arabidopsis J Plant Physiol* **188**, 44-48
31. Chakravorty, D., and Assmann, S. M. (2018) G protein subunit phosphorylation as a regulatory mechanism in heterotrimeric G protein signaling in mammals, yeast, and plants *Biochemical Journal* **475**, 3331-3357
32. Jones, J. C., Duffy, J. W., Machius, M., Temple, B. R. S., Dohlman, H. G., and Jones, A. M. (2011) The Crystal Structure of a Self-Activating G Protein α Subunit Reveals Its Distinct Mechanism of Signal Initiation *Sci Signal* **4**, ra8

33. Urano, D., Jones, J. C., Wang, H., Matthews, M., Bradford, W., Bennetzen, J. L. *et al.* (2012) G Protein Activation without a GEF in the Plant Kingdom *PLoS Genet* **8**, e1002756
34. Schmidt, T. G. M., and Skerra, A. (2007) The Strep-tag system for one-step purification and high-affinity detection or capturing of proteins *Nat Protoc* **2**, 1528-1535
35. Schmidt, T. G., and Skerra, A. (1993) The random peptide library-assisted engineering of a C-terminal affinity peptide, useful for the detection and purification of a functional Ig Fv fragment *Protein Eng* **6**, 109-122
36. Schmidt, T. G. M., Batz, L., Bonet, L., Carl, U., Holzapfel, G., Kiem, K. *et al.* (2013) Development of the Twin-Strep-tag® and its application for purification of recombinant proteins from cell culture supernatants *Protein Expr Purif* **92**, 54-61
37. Schmidt, T. G. M., Koepke, J., Frank, R., and Skerra, A. (1996) Molecular Interaction Between the Strep-tag Affinity Peptide and its Cognate Target, Streptavidin *J Mol Biol* **255**, 753-766
38. McEwen, D. P., Gee, K. R., Kang, H. C., and Neubig, R. R. (2001) Fluorescent BODIPY-GTP Analogs: Real-Time Measurement of Nucleotide Binding to G Proteins *Analytical Biochemistry* **291**, 109-117
39. Willard, F. S., Kimple, A. J., Johnston, C. A., and Siderovski, D. P. (2005) A direct fluorescence-based assay for RGS domain GTPase accelerating activity *Analytical Biochemistry* **340**, 341-351
40. Jameson, E. E., Roof, R. A., Whorton, M. R., Mosberg, H. I., Sunahara, R. K., Neubig, R. R. *et al.* (2005) Real-time Detection of Basal and Stimulated G Protein GTPase Activity Using Fluorescent GTP Analogues *J Biol Chem* **280**, 7712-7719
41. Maruta, N., Trusov, Y., Chakravorty, D., Urano, D., Assmann, S. M., and Botella, J. R. (2019) Nucleotide exchange-dependent and nucleotide exchange-independent functions of plant heterotrimeric GTP-binding proteins *Sci Signal* **12**, eaav9526
42. Solis, G. P., Kozhanova, T. V., Koval, A., Zhilina, S. S., Mescheryakova, T. I., Abramov, A. A. *et al.* (2021) Pediatric Encephalopathy: Clinical, Biochemical and Cellular Insights into the Role of Gln52 of *GNAO1* and *GNAI1* for the Dominant Disease *Cells* **10**, 2749
43. Jeong, Y., and Chung, K. Y. (2023) Structural and Functional Implication of Natural Variants of Gαs *Int J Mol Sci* **24**, 4064
44. Barthel, T. K., and Walker, G. C. (1999) Inferences Concerning the ATPase Properties of DnaK and Other HSP70s Are Affected by the ADP Kinase Activity of Copurifying Nucleoside-diphosphate Kinase * *J Biol Chem* **274**, 36670-36678
45. Hauptmann, A., Podgoršek, K., Kuzman, D., Srčič, S., Hoelzl, G., and Loerting, T. (2018) Impact of Buffer, Protein Concentration and Sucrose Addition on the Aggregation and Particle Formation during Freezing and Thawing *Pharmaceutical Research* **35**, 101
46. Willard, F. S., and Siderovski, D. P. (2004) Purification and *In Vitro* Functional Analysis of the *Arabidopsis thaliana* Regulator of G-Protein Signaling-1 In Regulators of G-Protein Signaling, Part A, 320-338
47. Jones, J. C., Temple, B. R. S., Jones, A. M., and Dohlman, H. G. (2011) Functional Reconstitution of an Atypical G Protein Heterotrimer and Regulator of G Protein Signaling Protein (RGS1) from *Arabidopsis thaliana J Biol Chem* **286**, 13143-13150
48. Kleuss, C., Raw, A. S., Lee, E., Sprang, S. R., and Gilman, A. G. (1994) Mechanism of GTP hydrolysis by G-protein α subunits *Proc Natl Acad Sci U S A* **91**, 9828-9831
49. Wall, M. A., Posner, B. A., and Sprang, S. R. (1998) Structural basis of activity and subunit recognition in G protein heterotrimers *Structure with Folding & Design* **6**, 1169-1183
50. Gao, X., Du, Z., and Patel, T. B. (2005) Copper and Zinc Inhibit $G\alpha_s$ Function: A Nucleotide-free State of $G\alpha_s$ Induced by Cu^{2+} and Zn^{2+} *J Biol Chem* **280**, 2579-2586

51. Weinstein, L. S., and Shenker, A. (1993) G Protein Mutations in Human Disease *Clin Biochem* **26**, 333-338
52. Dror, R. O., Mildorf, T. J., Hilger, D., Manglik, A., Borhani, D. W., Arlow, D. H. *et al.* (2015) Structural basis for nucleotide exchange in heterotrimeric G proteins *Science* **348**, 1361-1365
53. Mafi, A., Kim, S.-K., and Goddard, W. A. (2022) The mechanism for ligand activation of the GPCR–G protein complex *Proc Natl Acad Sci U S A* **119**, e2110085119
54. Johnston, C. A., Taylor, J. P., Gao, Y., Kimple, A. J., Grigston, J. C., Chen, J. G. *et al.* (2007) GTPase acceleration as the rate-limiting step in *Arabidopsis* G protein-coupled sugar signaling *Proc Natl Acad Sci U S A* **104**, 17317-17322
55. Landrum, M. J., Lee, J. M., Riley, G. R., Jang, W., Rubinstein, W. S., Church, D. M. *et al.* (2013) ClinVar: public archive of relationships among sequence variation and human phenotype *Nucleic Acids Res* **42**, D980-D985
56. Tate, J. G., Bamford, S., Jubb, H. C., Sondka, Z., Beare, D. M., Bindal, N. *et al.* (2018) COSMIC: the Catalogue Of Somatic Mutations In Cancer *Nucleic Acids Res* **47**, D941-D947
57. Silva-Rodríguez, P., Fernández-Díaz, D., Bande, M., Pardo, M., Loidi, L., and Blanco-Teijeiro, M. J. (2022) GNAQ and GNA11 Genes: A Comprehensive Review on Oncogenesis, Prognosis and Therapeutic Opportunities in Uveal Melanoma *Cancers* **14**, 3066
58. John, J., Rensland, H., Schlichting, I., Vetter, I., Borasio, G. D., Goody, R. S. *et al.* (1993) Kinetic and Structural Analysis of the Mg^{2+}-binding Site of the Guanine Nucleotide-binding Protein $p21^{H\text{-}ras}$ *J Biol Chem* **268**, 923-929
59. Slepak, V. Z., Quick, M. W., Aragay, A. M., Davidson, N., Lester, H. A., and Simon, M. I. (1993) Random Mutagenesis of G protein α Subunit $G_o\alpha$ - Mutations Altering Nucleotide Binding *J Biol Chem* **268**, 21889-21894
60. Natochin, M., Barren, B., and Artemyev, N. O. (2006) Dominant Negative Mutants of Transducin-α That Block Activated Receptor *Biochemistry* **45**, 6488-6494
61. Ramachandran, S., and Cerione, R. A. (2011) A Dominant-negative Gα Mutant That Traps a Stable Rhodopsin-Gα-GTP-$\beta\gamma$ Complex *J Biol Chem* **286**, 12702–12711
62. Jones, J. C., Jones, A. M., Temple, B. R. S., and Dohlman, H. G. (2012) Differences in intradomain and interdomain motion confer distinct activation properties to structurally similar Gα proteins *Proc Natl Acad Sci U S A* **109**, 7275-7279
63. Rasmussen, S. G. F., DeVree, B. T., Zou, Y. Z., Kruse, A. C., Chung, K. Y., Kobilka, T. S. *et al.* (2011) Crystal structure of the β_2 adrenergic receptor-Gs protein complex *Nature* **477**, 549-555
64. Westfield, G. H., Rasmussen, S. G. F., Su, M., Dutta, S., DeVree, B. T., Chung, K. Y. *et al.* (2011) Structural flexibility of the Gαs α-helical domain in the β_2-adrenoceptor Gs complex *Proc Natl Acad Sci U S A* **108**, 16086-16091
65. Dorn, M., Jurk, M., and Schmieder, P. (2012) Blue News Update: BODIPY-GTP Binds to the Blue-Light Receptor YtvA While GTP Does Not *PLoS One* **7**, e29201
66. Goody, R. S. (2014) How not to do kinetics: examples involving GTPases and guanine nucleotide exchange factors *Febs J* **281**, 593-600
67. Skiba, N. P., Bae, H., and Hamm, H. E. (1996) Mapping of Effector Binding Sites of Transducin α-Subunit Using $G\alpha_t/G\alpha_{i1}$ Chimeras *J Biol Chem* **271**, 413-424
68. Slep, K. C., Kercher, M. A., He, W., Cowan, C. W., Wensel, T. G., and Sigler, P. B. (2001) Structural determinants for regulation of phosphodiesterase by a G protein at 2.0 Å *Nature* **409**, 1071-1077

69. Kreutz, B., Yau, D. M., Nance, M. R., Tanabe, S., Tesmer, J. J. G., and Kozasa, T. (2006) A New Approach to Producing Functional Gα Subunits Yields the Activated and Deactivated Structures of Gα12/13 Proteins *Biochemistry* **45**, 167-174
70. Angov, E., Hillier, C. J., Kincaid, R. L., and Lyon, J. A. (2008) Heterologous Protein Expression Is Enhanced by Harmonizing the Codon Usage Frequencies of the Target Gene with those of the Expression Host *PLoS One* **3**, e2189
71. Trehan, A., Kiełbus, M., Czapinski, J., Stepulak, A., Huhtaniemi, I., and Rivero-Müller, A. (2016) REPLACR-mutagenesis, a one-step method for site-directed mutagenesis by recombineering *Sci Rep* **6**, 19121
72. Ling, M. M., and Robinson, B. H. (1997) Approaches to DNA Mutagenesis: An Overview *Analytical Biochemistry* **254**, 157-178
73. Biggar, K. K., Dawson, N. J., and Storey, K. B. (2012) Real-time protein unfolding: a method for determining the kinetics of native protein denaturation using a quantitative real-time thermocycler *Biotechniques* **53**, 231-238

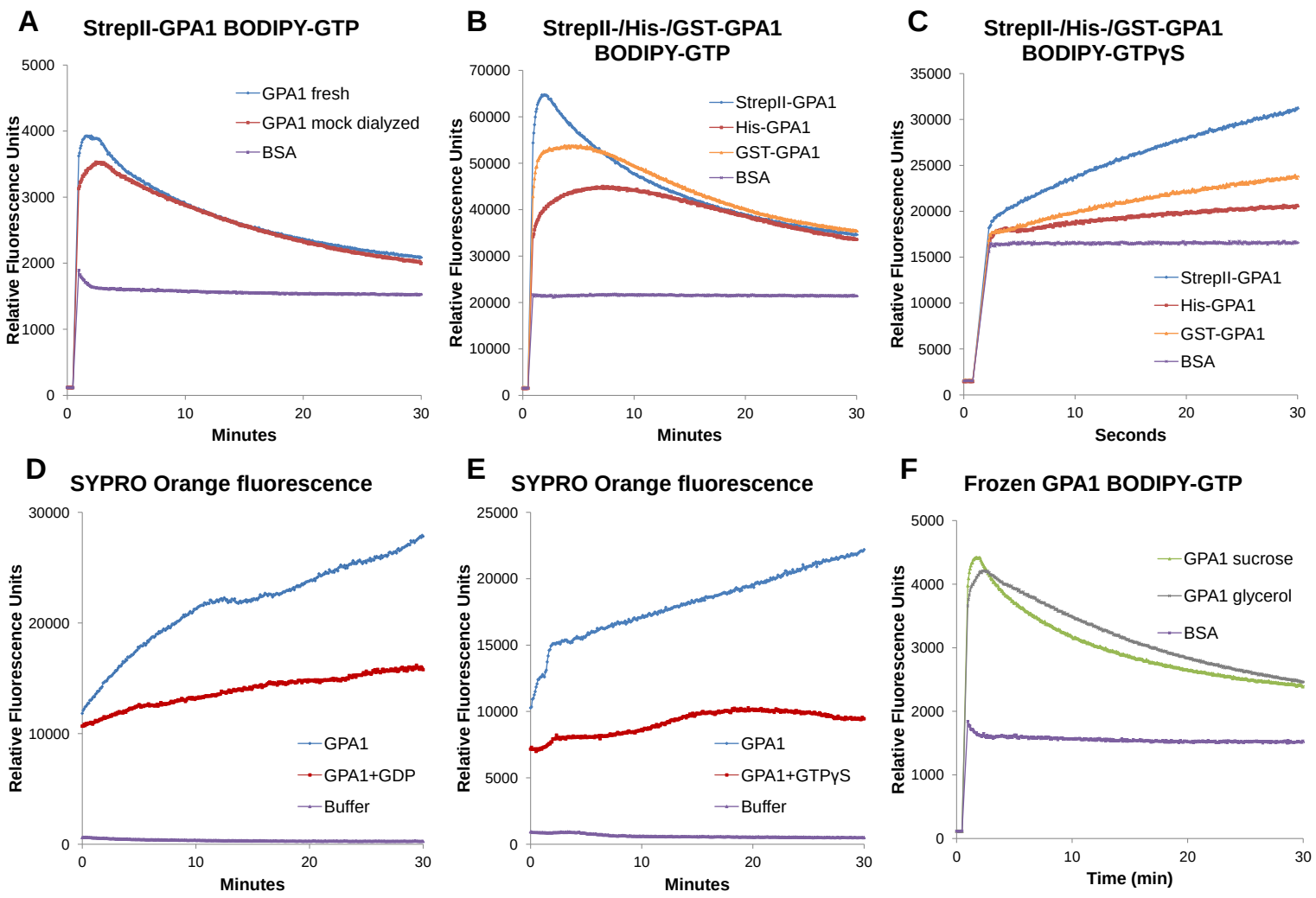

Figure 1. Fresh StrepII-tagged protein displays higher enzymatic activity than GPA1 proteins purified using other methods or that have been stored. **A.** BODIPY-GTP binding and hydrolysis curves of GPA1 either freshly prepared or subjected to overnight storage at 4 °C to simulate the temperature and time effect of dialysis. **B.** Comparison of BODIPY-GTP binding and hydrolysis of GPA1 isolated by StrepII-, His- and GST-tag purification procedures. **C.** Comparison of the initial binding rates (note x-axis units) of the samples in panel **B** when assayed with BODIPY-GTPγS. **D-E.** SYPRO Orange protein unfolding assays conducted at 25 °C with GPA1 in the absence of additional nucleotides, compared to GPA1 supplemented with **D.** 125 µM GDP or **E.** 125 µM GTPγS. **F.** Comparison of BODIPY-GTP binding and hydrolysis activities of StrepII-GPA1 stored at -80 °C for 3 weeks with either 10% glycerol or 8.33% sucrose added to the elution fraction (which contains 5% glycerol) as a cryoprotectant. Note: For assays depicted in panels **A** and **F** the detector gain was set to 70, as opposed to 90-100 for other assays, hence the lower relative fluorescence values. 100 nM protein was used in BODIPY assays and 600 nM protein in SYPRO Orange assays.

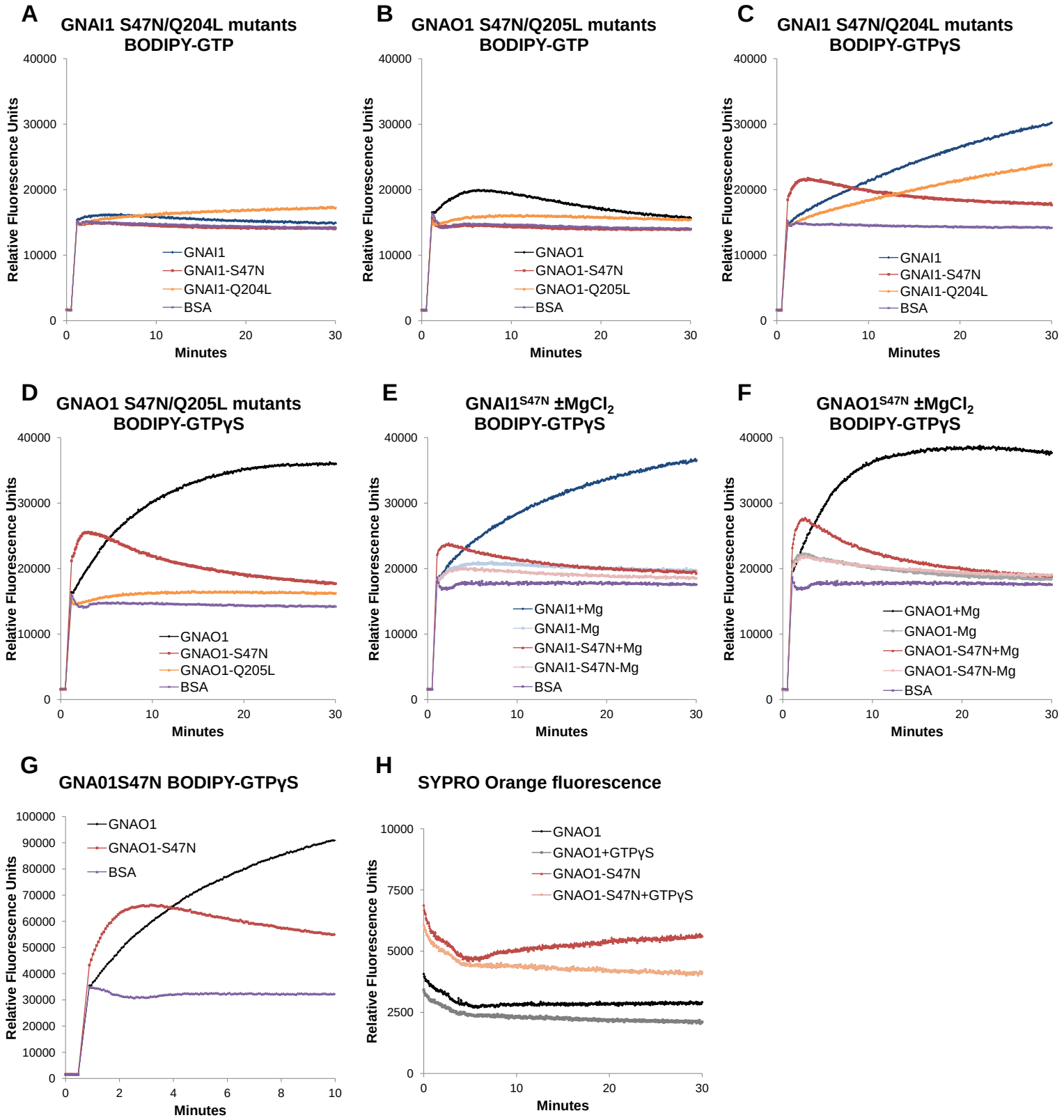

Figure 2. Comparison of StrepII-GNAI1 and StrepII-GNAO1 with dominant negative (S47N) and constitutively active (Q204L/Q205L) mutants. **A-B.** BODIPY-GTP binding and hydrolysis curves of **A.** GNAI1 or **B.** GNAO1, with corresponding mutants. **C-D.** BODIPY-GTPγS binding curves of **C.** GNAI1 or **D.** GNAO1, with corresponding mutants. **E-F.** Mg^{2+} dependency assays for BODIPY-GTPγS binding by **E.** GNAI1 vs. $GNAI1^{S47N}$ or **F.** GNAO1 vs. $GNAO1^{S47N}$. Note: all proteins assayed in panels **A-F** had been stored at -80 °C with 8.33% sucrose added as a cryoprotectant. **G.** BODIPY-GTPγS binding curves for freshly prepared GNAO1 vs. $GNAO1^{S47N}$ over a 10 min time course. **H.** SYPRO Orange protein unfolding assay of freshly prepared GNAO1 vs. $GNAO1^{S47N}$. Note the expanded y-axis scale. The initial decrease in SYPRO Orange signal may result from temperature equilibration, as reactions were loaded immediately following sample preparation on ice.200 nM protein was used in GNAI1 and 100 nM protein in GNAO1 BODIPY assays. 600 nM protein was used in the SYPRO Orange assay.

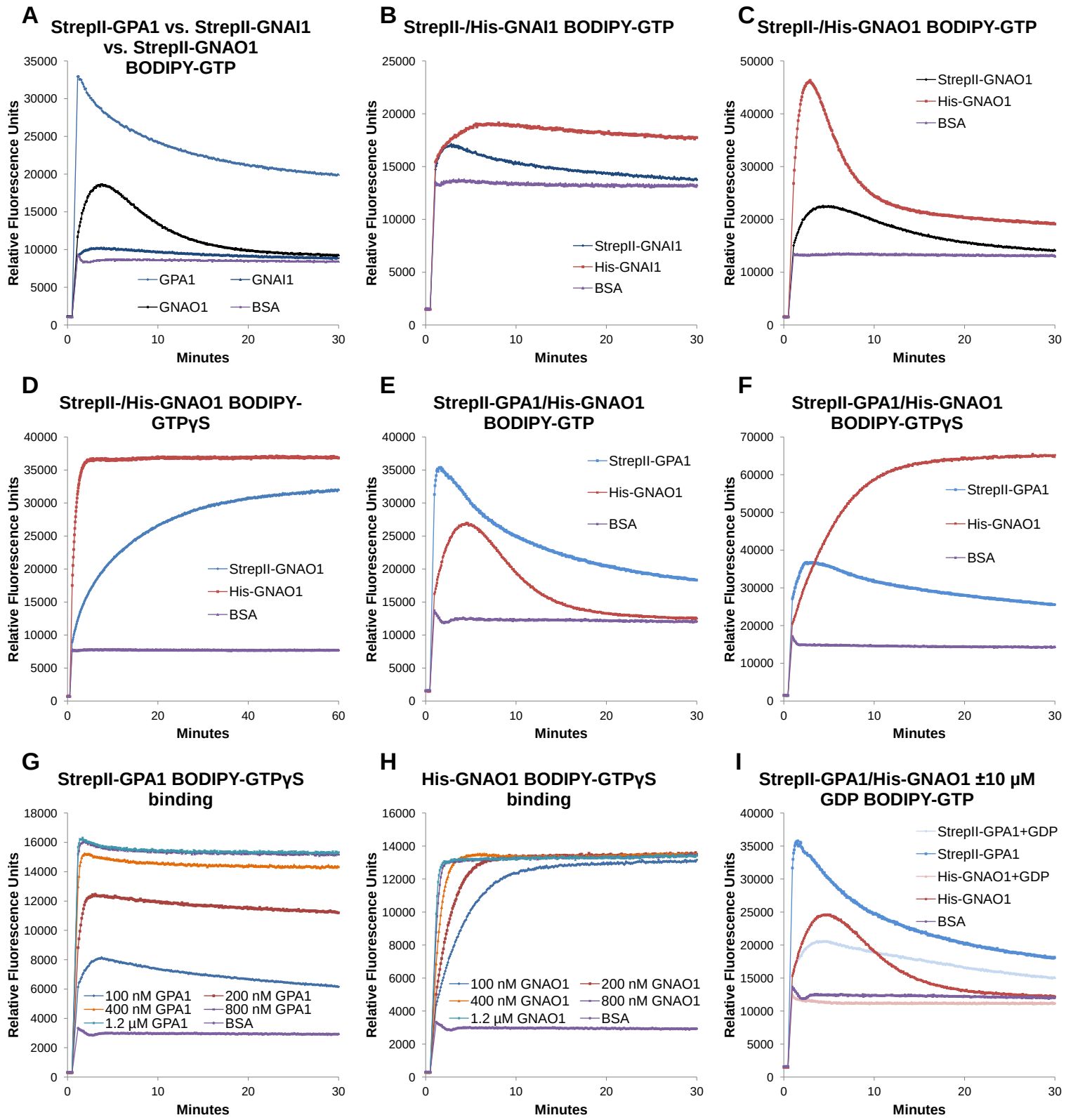

Figure 3. Comparison of GPA1 activity to GNAI1 and GNAO1 activity. **A.** BODIPY-GTP binding and hydrolysis curves of StrepII-GPA1, StrepII-GNAI1 and StrepII-GNAO1. **B-C.** BODIPY-GTP binding and hydrolysis curves of **B.** StrepII-GNAI1 vs. His-GNAI1 and **C.** StrepII-GNAO1 vs. His-GNAO1. **D.** BODIPY-GTPγS binding curves of StrepII-GPA1 vs. His-GNAO1. **E-F.** Comparison of enzyme kinetics of StrepII-GPA1 vs. His-GNAO1. **E.** Binding and hydrolysis of BODIPY-GTP or **F.** binding of BODIPY-GTPγS. **G-H.** Concentration-dependent kinetics and maximal binding of BODIPY-GTPγS by **G.** StrepII-GPA1 or **H.** His-GNAO1. **I.** Comparison of binding and hydrolysis of BODIPY-GTP by StrepII-GPA1 vs. His-GNAO1 ±10 µM GDP. Gα proteins were used at 220 nM in panel B and 130 nM protein in panels C and D, while 100 nM protein was used in panels A, E, F and I.

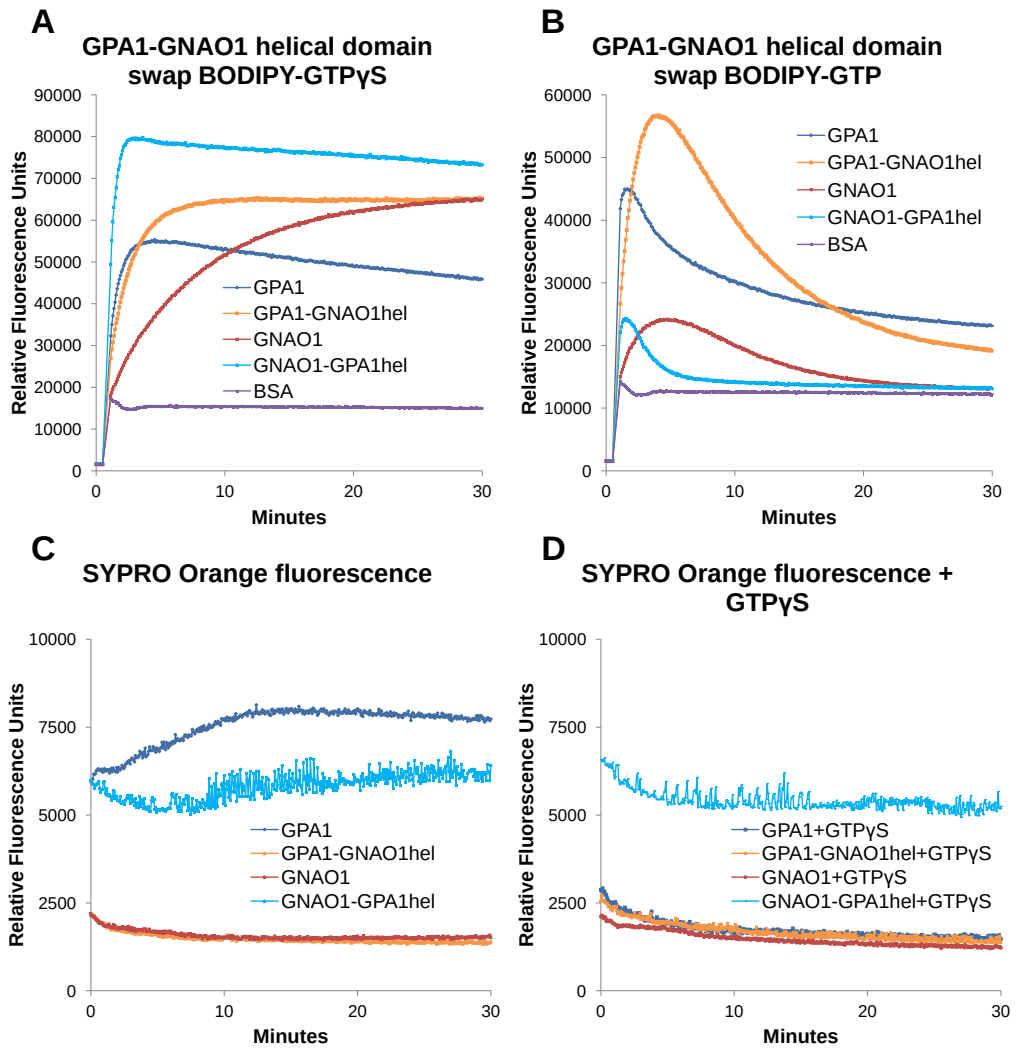

Figure 4. Helical domain swap between GPA1 and GNAO1. Regions encoding the helical domains of GPA1 (residues 68-188) and GNAO1 (residues 63-177) were reciprocally swapped by overlap-extension PCR and the resultant constructs were all expressed with dual StrepII-tags, to eliminate the tag as a variable. **A-B.** Curves of GPA1, GNAO1 and helical domain swaps for **A.** BODIPY-GTPγS binding and **B.** BODIPY-GTP binding and hydrolysis**C-D.** SYPRO Orange protein unfolding assays conducted at 25 °C with GPA1, GNAO1, $GPA1^{GNAO1hel}$ or $GNAO1^{GPA1hel}$ **C.** without additional nucleotides, or **D.** in the presence of ±10 µM GTPγS. 100 nM protein was used in BODIPY assays and 400 nM protein in SYPRO Orange assays.